Pre-Equalization for Pre-Rake MISO DS-UWB Systems*

Elham Torabi, Jan Mietzner, and Robert Schober

Dept. of Elec. & Comp. Engineering, The University of British Columbia, 2332 Main Mall, Vancouver, BC, V6T 1Z4, Canada.
E-mail: {elhamt,janm,rschober}@ece.ubc.ca.

***Abstract*— In this paper, we propose two novel pre–equalization schemes for multiple–input single–output (MISO) direct–sequence ultra–wideband (DS–UWB) systems with pre–Rake combining and symbol–by–symbol detection. The first pre–equalization filter (PEF) scheme employs one PEF per transmit antenna, whereas in the second, simplified PEF (S–PEF) scheme all transmit antennas share the same PEF. For both schemes, the optimum finite impulse response (FIR) and infinite impulse response (IIR) PEFs are calculated based on the minimum mean squared error (MMSE) criterion. Our approach is sufficiently general to include also complexity–reduced versions of pre–Rake combining that employ a limited number of Rake fingers. We show that under certain conditions the S–PEF scheme achieves the same performance as the more complex PEF scheme. Moreover, our simulation results show that the proposed PEF schemes achieve significant performance gains over pure pre–Rake combining without equalization, even if only short PEFs are employed.**

I. Introduction

In recent years, ultra–wideband (UWB) signaling has emerged as a promising solution to high–rate short–range wireless personal area networks. Due to their extremely large bandwidths, UWB systems can resolve even dense multipath components, such that Rake combining can be used at the receiver to significantly reduce the negative effects of fading in the received signal [1]. However, for many UWB applications the receiver is a portable device with severely limited signal processing capabilities, rendering Rake combiners with a sufficiently large number of fingers very challenging.

A promising approach to overcome this problem is to move computational complexity from the receiver to the more powerful transmitter (e.g. an access point). For this purpose, the concept of pre–Rake combining (also referred to as time–reversal transmission) was borrowed from other areas, such as time–division duplex code–division multiple access (TDD–CDMA) systems [2] and underwater acoustic communication [3], and was modified for UWB applications, e.g. [4]–[8]. Pre–Rake combining exploits the reciprocity of the UWB channel, which was recently experimentally confirmed in [7]. Ideally, with pre–Rake combining channel estimation, diversity combining, and equalization are avoided at the receiver, and a simple symbol–by–symbol detector can be used [8]. In addition, it has been recently shown that pre–Rake combining also performs well in the presence of multiple users [5], and an extension to multiple–input single–output (MISO) scenarios was proposed in [5], [7].

Despite all of these desirable properties, pre–Rake combining has a serious drawback. In particular, for the long channel impulse responses (CIRs), which are typical for UWB applications, it may entail a relatively high error floor, if simple symbol–by–symbol detection is applied at the receiver. To remedy this problem, receiver–side equalization [4] and post–Rake combining [6] have been proposed. However, these techniques increase the receiver complexity and thus compromise to some extend the advantages of pre–Rake combining. Therefore, transmitter–side approaches for performance improvement seem to be more suitable for pre–Rake UWB systems. One option in this regard is to decrease the data rate (i.e., increase the chip or/and symbol duration), which effectively decreases the residual intersymbol interference (ISI) at the receiver [8]. However, if high data rates are desired, some form of pre–equalization has to be applied at the transmitter. In [9] the pre–Rake filter is replaced by a pre–filter which minimizes the residual ISI at the receiver based on the minimum mean squared error (MMSE) criterion. Since this MMSE pre–filter is implemented at the chip level, depending on the underlying channel relatively long filters may be necessary, in order to achieve a good performance. This entails a high complexity, since the computation of the filter coefficients requires the inversion of a matrix of size equal to the filter length.

In this paper, we propose a novel pre–equalization filter (PEF) scheme for MISO direct–sequence (DS) UWB systems, which consists of a bank of pre–Rake filters and a bank of PEFs. Unlike [9], we retain the pre–Rake filters, as they efficiently shorten the overall CIRs, and implement the PEFs at the symbol level. Although pre–equalization problems have been extensively studied in the literature, e.g. [10], existing results cannot be easily adopted for the problem at hand, due to the presence of the pre–Rake filter, the imposed simple receiver processing, and the spreading applied in DS–UWB. Consequently, in this paper, we derive the optimum finite impulse response (FIR) and infinite impulse response (IIR) MMSE PEFs and analyze the performance of the resulting system. Furthermore, we also study a simplified PEF (S–PEF) scheme, where the bank of PEFs is replaced by a single PEF that is shared by all antennas. Our approach is sufficiently general to include also complexity–reduced versions of pre–Rake combining that employ a limited number of Rake fingers. We demonstrate that, under certain conditions, the S–PEF scheme can achieve the same performance as the more complex PEF scheme. Our simulation results confirm that the proposed PEF schemes achieve significant performance gains over pure pre–Rake structures without equalization, and that the performance of IIR PEFs can be closely approached by relatively short FIR PEFs.

Paper organization: In Section II, we present the considered system and channel model. The proposed PEF scheme is optimized and analyzed in Section III, and the S–PEF scheme is investigated in Section IV. In Section V, simulation results are provided, and Section VI concludes this paper.

Notation: $\mathcal{E}\{\cdot\}$, $[\cdot]^T$, $(\cdot)^*$, $[\cdot]^H$, and $\mathrm{diag}\{\cdot\}$ denote statistical expectation, transposition, complex conjugation, Hermitian transposition, and a (block) diagonal matrix, respectively. $\mathbf{0}_X$, $\boldsymbol{e}_n$, $\Re\{\cdot\}$, and $*$ stand for the X–dimensional all–zeros column vector, the unit vector whose elements are all zero except for the nth element which is equal to 1, the real part of a complex number, and linear convolution, respectively. Furthermore, $Q(x) \triangleq \frac{1}{\sqrt{2\pi}} \int_x^\infty e^{-t^2/2}\,\mathrm{d}t$, $\delta(\cdot)$, and $X(e^{j\omega}) \triangleq \mathcal{F}\{x[k]\} = \sum_{k=-\infty}^{\infty} x[k]e^{-j\omega k}$ denote the Gaussian Q–function, the Dirac delta function, and the discrete–time Fourier transform of $x[k]$, respectively.

* This work was partly supported by a postdoctoral fellowship from the German Academic Exchange Service (DAAD).

II. System and Channel Model

We consider a MISO DS–UWB system with M transmit antennas, symbol duration T_s, and chip duration $T_c = T_s/N$, where N is the spreading factor. A block diagram of the discrete–time model of this system is shown in Fig. 1. We note that our results could be extended to multiple receive antennas in a straightforward fashion. However, for the sake of clarity and since a simple receiver structure is desired, we assume that only a single receive antenna is available. For convenience, all signals and systems are represented by their complex baseband equivalents.

Transmitter structure: At antenna m, $1 \le m \le M$, the transmitted independent and identically distributed (i.i.d.) data symbols $a[n] \in \{\pm 1\}$ are filtered with a PEF $f_m[n]$ of length L_f, and the filter output signal $v_m[n] \triangleq f_m[n] * a[n]$ is up–sampled by a factor of N. The up–sampled signal is then filtered with a (real–valued) spreading sequence $c[k]$, $0 \le k < N$, and with a pre–Rake filter $g_m[k]$ of length L_g. For convenience, the spreading sequence is normalized to $\sum_{k=0}^{N-1} |c[k]|^2 = 1$. The resulting transmit symbol $s_m[k]$ is given by

$$s_m[k] = \sum_{i=-\infty}^{\infty} v_m[i]\tilde{g}_m[k - iN], \tag{1}$$

where $\tilde{g}_m[k] \triangleq c[k] * g_m[k]$ includes the combined effects of the pre–Rake filter and spreading. We note that the considered transmitter structure is very general, since we do not impose any restrictions on $c[k]$ and $g_m[k]$. If a spreading sequence is not applied, e.g. [4], [9], we have $c[0] = 1$ and $c[k] = 0$, $1 \le k < N$. In general, $g_m[k]$, $1 \le m \le M$, will depend in some way on the CIR $h_m[k]$, which has length L_h. For example, an all–pre–Rake (A–pre–Rake or time–reversal) filter $g_m[k] \triangleq h_m^*[L_h - k - 1]$, $0 \le k < L_g$ ($L_g = L_h$) may be adopted, or a selective pre–Rake (S–pre–Rake) filter, with $g_m[k] \triangleq h_m^*[L_g - k - 1]$ for the S largest coefficients of $h_m[k]$ and $g_m[k] \triangleq 0$ otherwise ($L_g \le L_h$). Due to the reciprocity of UWB channels [7], $h_m[k]$ can be estimated at the transmitter, thus relieving the receiver from any channel estimation tasks.

Channel model: The equivalent baseband discrete–time CIRs $h_m[k] \triangleq g_T(t) * h_m(t) * g_R(t)|_{kT_c}$, $1 \le m \le M$, contain the combined effects of the transmit filter $g_T(t)$, the continuous–time CIR $h_m(t)$, and the receive filter $g_R(t)$. For convenience and practical relevance, we use in this paper the parameters from the IEEE 802.15.3a standardization efforts. In particular, a chip duration of $T_c = 0.76$ ns is adopted, and both $g_T(t)$ and $g_R(t)$ are square–root raised–cosine filters with roll–off factor 0.3 [11]. Furthermore, for the wireless channel we adopt the recently proposed extension of the IEEE 802.15.3a channel model [12] to multiple antennas [13]. Consequently, the passband version $h'_m(t)$ of the baseband CIR $h_m(t)$ consists of L_c clusters of L_r rays and is modeled as

$$h'_m(t) = X_m \sum_{l=1}^{L_c} \sum_{k=1}^{L_r} \alpha_{k,l,m}\delta(t - T_{l,m} - \tau_{k,l,m}), \tag{2}$$

where $T_{l,m}$ is the delay of the lth cluster, $\tau_{k,l,m}$ is the delay of the kth ray of the lth cluster, $\alpha_{k,l,m}$ is the corresponding random multipath gain coefficient, and X_m models lognormal shadowing. Measurements reported in [13] have confirmed that while $T_{l,m}$, $\tau_{k,l,m}$, and $\alpha_{k,l,m}$ are independent across antennas, the lognormal terms X_m are mutually correlated. In [12] four parameter sets for the various channel model parameters in (2) are specified. The resulting four channel models (CMs) are known as CM1 – CM4 and represent different usage scenarios (associated with different amounts of ISI).

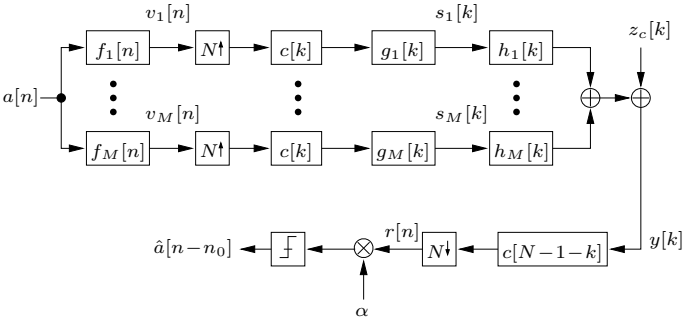

Fig. 1. Block diagram of a MISO DS–UWB system with M transmit antennas, pre–Rake combining, and pre–equalization.

Receiver structure: The received signal $y[k]$ is filtered with the time–reversed spreading sequence $c[N-1-k]$, $0 \le k < N$, and is then sampled at times $k = Nn + k_0$, where $0 \le k_0 < N$ denotes the sampling phase. The resulting received signal $r[n]$ can be expressed as

$$r[n] = \sum_{m=1}^{M} \sum_{l=-\infty}^{\infty} q_m[Nl + k_0]v_m[n - l] + z_s[n], \tag{3}$$

where $q_m[k] \triangleq \tilde{g}_m[k] * \tilde{h}_m[k]$, $\tilde{h}_m[k] \triangleq h_m[k] * c[N-1-k]$, denotes the overall CIR, and $z_s[n] = \sum_{i=0}^{N-1} c[i]z_c[N(n-1) + k_0 + i + 1]$ the symbol–level noise, while $z_c[k]$ denotes the chip–level additive white Gaussian noise (AWGN) with variance $\sigma_c^2 \triangleq \mathcal{E}\{|z_c[k]|^2\}$. Consequently, $z_s[n]$ is also AWGN with variance $\sigma_s^2 \triangleq \mathcal{E}\{|z_s[n]|^2\} = \sigma_c^2$. The sampling phase k_0 is optimized to maximize the energy $\sum_{l=-\infty}^{\infty} |q_m[Nl + k_0]|^2$ of the overall CIR. The optimum value for k_0 depends on L_g and L_h. Since the goal of the proposed UWB system design is to minimize the receiver complexity, $r[n]$ is only multiplied with a constant gain α, before a decision is made according to

$$\hat{a}[n - n_0] = \text{sign}\,\{\Re\{\alpha r[n]\}\}, \tag{4}$$

where $\hat{a}[n-n_0]$ is the estimate for $a[n-n_0]$, n_0 denotes the decision delay, and $\text{sign}\,\{x\} = 1$ if $x \ge 0$ and $\text{sign}\,\{x\} = -1$ otherwise. As typical for equalization problems, the decision delay n_0 has to be optimized, if causal pre–filters are desired. As will be seen in Section III, α can be chosen as $\alpha > 0$ without loss of generality, i.e., the multiplication with α in (4) is not necessary and does not have to be implemented at the receiver. However, α simplifies the optimization of the PEFs $f_m[n]$ and may thus be thought of as an auxiliary variable.

III. PEF Optimization and Performance Analysis

Throughout this paper we focus on a single-user scenario. In the sequel, we adopt the MMSE criterion for optimization of the PEFs $f_m[n]$ and α. In particular, our design goal is to minimize the error variance

$$\sigma_e^2 \triangleq \mathcal{E}\{|a[n-n_0] - \alpha r[n]|^2\}, \tag{5}$$

while limiting the power P of the transmitted signals over one symbol interval, i.e.,

$$P \triangleq \sum_{k=Nn}^{N(n+1)-1} \sum_{m=1}^{M} \mathcal{E}\{|s_m[k]|^2\} = 1, \qquad \forall n. \tag{6}$$

In the following subsections, we will derive the optimum FIR and IIR PEFs based on (5), (6) and analyze their performance.

A. FIR Pre–Equalization Filters

For FIR PEF optimization, it is convenient to first rewrite (3) as

$$r[n]=\sum_{m=1}^{M}(\boldsymbol{Q}_m\boldsymbol{f}_m)^H\boldsymbol{a}[n]+z_s[n]=(\boldsymbol{Q}\boldsymbol{f})^H\boldsymbol{a}[n]+z_s[n], \quad (7)$$

where $\boldsymbol{a}[n]\triangleq[a[n]\ \dots\ a[n-L_t+1]]^T$, $\boldsymbol{f}\triangleq[\boldsymbol{f}_1^T\ \dots\ \boldsymbol{f}_M^T]^T$, $\boldsymbol{f}_m\triangleq[f_m[0]\ \dots\ f_m[L_f-1]]^H$, $\boldsymbol{Q}\triangleq[\boldsymbol{Q}_1\ \dots\ \boldsymbol{Q}_M]$, and $\boldsymbol{Q}_m$ denotes an $L_t\times L_f$ column–circulant matrix with vector $[q_m[k_0]\ q_m[N+k_0]\ \dots\ q_m[N(L_q-1)+k_0]\ \boldsymbol{0}_{L_f-1}^T]^H$ as first column. Here, $L_t\triangleq L_q+L_f-1$ is the length of the impulse response of the overall system (including the PEFs), where $L_q=\lceil(L_g+L_h+2N-3)/N\rceil$ is the length of the sampled overall CIR $q_m[Nn+k_0]$. Applying (7) in (5) yields

$$\sigma_e^2=1+|\alpha|^2\sigma_c^2-\alpha\boldsymbol{f}^H\boldsymbol{q}-\alpha^*\boldsymbol{q}^H\boldsymbol{f}+|\alpha|^2\boldsymbol{f}^H\boldsymbol{Q}^H\boldsymbol{Q}\boldsymbol{f}, \quad (8)$$

where $\boldsymbol{q}\triangleq\boldsymbol{Q}^H\boldsymbol{e}_{n_0}$. Furthermore, it can be shown that the average transmit power P in (6) can be expressed as

$$P=\boldsymbol{f}^H\boldsymbol{\Phi}\boldsymbol{f}, \quad (9)$$

where $\boldsymbol{\Phi}\triangleq\mathrm{diag}\{\boldsymbol{\Phi}_1,\dots,\boldsymbol{\Phi}_M\}$ is an $ML_f\times ML_f$ block diagonal matrix consisting of symmetric Toeplitz matrices $\boldsymbol{\Phi}_m$ with vector $[\varphi_m[0]\ \varphi_m[-N]\ \dots\ \varphi_m[-N(L_f-1)]]$ in the first row, while $\varphi_m[k]\triangleq\tilde{g}_m[k]*\tilde{g}_m^*[-k]$. Combining (8) and (9), we obtain the Lagrange problem $L(\boldsymbol{f},\alpha)\triangleq\sigma_e^2+\lambda(P-1)$, where λ denotes the Lagrange multiplier. Differentiating $L(\boldsymbol{f},\alpha)$ with respect to $\boldsymbol{f}^*$ and α^* and setting the resulting gradients to zero leads to the optimum solution

$$\begin{aligned}\boldsymbol{f}_{\mathrm{opt}} &= \frac{1}{\alpha_{\mathrm{opt}}^*}\left(\boldsymbol{Q}^H\boldsymbol{Q}+\sigma_c^2\boldsymbol{\Phi}\right)^{-1}\boldsymbol{q}, \quad (10)\\ \alpha_{\mathrm{opt}} &= \sqrt{\boldsymbol{q}^H\left(\boldsymbol{Q}^H\boldsymbol{Q}+\sigma_c^2\boldsymbol{\Phi}\right)^{-1}\boldsymbol{\Phi}\left(\boldsymbol{Q}^H\boldsymbol{Q}+\sigma_c^2\boldsymbol{\Phi}\right)^{-1}\boldsymbol{q}}.\end{aligned}$$

Using (10) in (8) leads to the minimum error variance

$$\sigma_{e,\min}^2=1-\boldsymbol{q}^H\left(\boldsymbol{Q}^H\boldsymbol{Q}+\sigma_c^2\boldsymbol{\Phi}\right)^{-1}\boldsymbol{q}. \quad (11)$$

Noting that the received signal can be expressed as

$$r[n]=\boldsymbol{f}^H\boldsymbol{q}a[n-n_0]+\boldsymbol{f}^H\boldsymbol{Q}^H\boldsymbol{a}_{n_0}[n]+z_s[n], \quad (12)$$

where $\boldsymbol{a}_{n_0}[n]$ is identical to $\boldsymbol{a}[n]$ except that its n_0th component is zero, we can find the following expression for the effective signal-to-noise ratio (SNR) at the receiver:

$$\mathrm{SNR}=\frac{|\boldsymbol{f}^H\boldsymbol{q}|^2}{\boldsymbol{f}^H\boldsymbol{Q}^H\boldsymbol{Q}\boldsymbol{f}-|\boldsymbol{f}^H\boldsymbol{q}|^2+\sigma_c^2}=\frac{1}{\sigma_{e,\min}^2}-1. \quad (13)$$

For calculation of $\boldsymbol{f}_{\mathrm{opt}}$, an $ML_f\times ML_f$ matrix has to be inverted, which is computationally expensive for large L_f. Therefore, from a complexity point of view, short FIR filters are desirable. On the other hand, the performance of the proposed pre–equalization scheme improves with increasing L_f. Therefore, we are interested in finding the minimum value of L_f which achieves close–to–optimum performance. In this context, the optimum IIR solution is useful, since it allows us to establish the ultimate performance limit of the proposed PEF scheme.

B. IIR Pre–Equalization Filters

As customary for IIR filter optimization, we drop the causality constraint and set $n_0=0$. Furthermore, we define $\boldsymbol{F}(e^{j\omega})\triangleq[F_1(e^{j\omega})\dots F_M(e^{j\omega})]^H$ as the vector of IIR PEF frequency responses, where $F_m(e^{j\omega})\triangleq\mathcal{F}\{f_m[n]\}$, and $\boldsymbol{Q}(e^{j\omega})\triangleq[Q_1(e^{j\omega})\dots Q_M(e^{j\omega})]^T$ as the vector of the Fourier transforms of the sampled overall CIRs $q_m[Nn+k_0]$, $1\le m\le M$, i.e., $Q_m(e^{j\omega})\triangleq\mathcal{F}\{q_m[Nn+k_0]\}$. Note that $Q_m(e^{j\omega})$ is related to the Fourier transform $\tilde{Q}_m(e^{j\omega})\triangleq\mathcal{F}\{q_m[k+k_0]\}$ of the (time-shifted) overall CIR itself via [14]

$$Q_m(e^{j\omega})=\frac{1}{N}\sum_{k=0}^{N-1}\tilde{Q}_m(e^{j(\omega-2\pi k)/N}). \quad (14)$$

With these definitions, the error variance (8) can be rewritten as

$$\begin{aligned}\sigma_e^2 &= 1+|\alpha|^2\sigma_c^2 \quad (15)\\ &- \frac{1}{2\pi}\int_{-\pi}^{\pi}\Big[\alpha\boldsymbol{F}^H(e^{j\omega})\boldsymbol{Q}(e^{j\omega})+\alpha^*\boldsymbol{Q}^H(e^{j\omega})\boldsymbol{F}(e^{j\omega})\\ &- |\alpha|^2\boldsymbol{F}^H(e^{j\omega})\boldsymbol{Q}(e^{j\omega})\boldsymbol{Q}^H(e^{j\omega})\boldsymbol{F}(e^{j\omega})\Big]\,\mathrm{d}\omega.\end{aligned}$$

Similarly, using the definition $\boldsymbol{\Phi}(e^{j\omega})\triangleq\mathrm{diag}\{\Phi_1(e^{j\omega}),\Phi_2(e^{j\omega}),\dots,\Phi_M(e^{j\omega})\}$, where $\Phi_m(e^{j\omega})\triangleq\mathcal{F}\{\varphi_m[Nn]\}$, the average transmit power in (9) can be expressed as

$$P=\frac{1}{2\pi}\int_{-\pi}^{\pi}\boldsymbol{F}^H(e^{j\omega})\boldsymbol{\Phi}(e^{j\omega})\boldsymbol{F}(e^{j\omega})\,\mathrm{d}\omega. \quad (16)$$

We note that the Fourier transform $\Phi_m(e^{j\omega})$ of the sampled sequence $\varphi_m[Nn]$ is related to the Fourier transform $\tilde{\Phi}_m(e^{j\omega})\triangleq\mathcal{F}\{\varphi_m[k]\}$ of the sequence $\varphi_m[k]$ itself by $\Phi_m(e^{j\omega})=\frac{1}{N}\sum_{k=0}^{N-1}\tilde{\Phi}_m(e^{j(\omega-2\pi k)/N})$ [14]. Based on (15) and (16) we can now formulate a similar Lagrange problem as in the FIR case. Furthermore, employing the matrix inversion lemma [15], we finally obtain the following optimal solution for the mth component of $\boldsymbol{F}(e^{j\omega})$:

$$\begin{aligned}F_m^{\mathrm{opt}}(e^{j\omega}) &= \frac{1}{\alpha_{\mathrm{opt}}^*}\frac{Q_m(e^{j\omega})}{\Phi_m(e^{j\omega})(\sigma_c^2+X(e^{j\omega}))}, \quad (17)\\ \alpha_{\mathrm{opt}} &= \sqrt{\frac{1}{2\pi}\int_{-\pi}^{\pi}\frac{X(e^{j\omega})}{(\sigma_c^2+X(e^{j\omega}))^2}\,\mathrm{d}\omega},\end{aligned}$$

$$X(e^{j\omega})=\boldsymbol{Q}^H(e^{j\omega})\boldsymbol{\Phi}^{-1}(e^{j\omega})\boldsymbol{Q}(e^{j\omega})=\sum_{m=1}^{M}\frac{|Q_m(e^{j\omega})|^2}{\Phi_m(e^{j\omega})}.$$

The corresponding minimum error variance can be obtained from (15) as

$$\sigma_{e,\min}^2=\frac{1}{2\pi}\int_{-\pi}^{\pi}\frac{\sigma_c^2}{\sigma_c^2+X(e^{j\omega})}\,\mathrm{d}\omega. \quad (18)$$

The effective SNR at the receiver is obtained based on (13), by using (18) instead of (11) for the error variance $\sigma_{e,\min}^2$.

C. Optimality of A-Pre-Rake Combining

It is well known that the performance of pre–Rake (and post–Rake) schemes does not necessarily improve when the number of Rake fingers is increased, cf. e.g. [16]. The reason for this

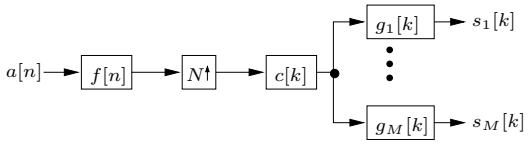

Fig. 2. Block diagram of a MISO DS–UWB system with M transmit antennas, pre–Rake combining, and simplified pre–equalization.

behavior is that while more energy can be collected by increasing the number of fingers, the amount of residual ISI may also increase. A similar effect can be observed, if the pre–Rake filter is enhanced with short FIR PEFs. However, we will show in the following that the A–pre–Rake (or time–reversal) filter is indeed optimum, if the PEFs are sufficiently long.

For this purpose, we focus on the IIR case and use (14) and the corresponding definition of $\Phi_m(e^{j\omega})$ to rewrite $X(e^{j\omega})$ as

$$X(e^{j\omega}) = \frac{1}{N}\sum_{m=1}^{M}\frac{B_m(e^{j\omega})}{\sum_{k=0}^{N-1}|\tilde{G}_m(e^{j(\omega-2\pi k)/N})|^2}, \qquad (19)$$

with $B_m(e^{j\omega}) \triangleq |\sum_{k=0}^{N-1}\tilde{G}_m(e^{j(\omega-2\pi k)/N})e^{j(\omega-2\pi k)k_0/N}\times \tilde{H}_m(e^{j(\omega-2\pi k)/N})|^2$, where we have used that $\tilde{Q}_m(e^{j\omega}) = e^{j\omega k_0}\tilde{G}_m(e^{j\omega})\tilde{H}_m(e^{j\omega})$, and $\tilde{\Phi}_m(e^{j\omega}) = |\tilde{G}_m(e^{j\omega})|^2$. Using the Cauchy–Schwarz inequality [15], it can be shown that $X(e^{j\omega})$ is maximized if $\tilde{G}_m(e^{j\omega}) = e^{-j\omega k_0}\tilde{H}_m^*(e^{j\omega})$, which corresponds to an A–pre–Rake filter for each branch m, $1 \le m \le M$. Therefore, the A–pre–Rake filter minimizes the error variance $\sigma^2_{e,\min}$ and is optimum, if IIR PEFs are employed. In particular, for an A–pre–Rake filter we obtain $X(e^{j\omega}) = \sum_{m=1}^{M}\psi_m(e^{j\omega})$, where $\psi_m(e^{j\omega}) \triangleq \frac{1}{N}\sum_{k=0}^{N-1}|\tilde{H}_m(e^{j(\omega-2\pi k)/N})|^2$. Increasing the spreading factor N improves performance by decreasing the effective spectral fluctuation for a given m, i.e., $\psi_m(e^{j\omega})$ becomes smoother over ω, which has a positive effect on $\sigma^2_{e,\min}$, cf. (18).

IV. Simplified PEF Structure

In this section, we consider a simplified PEF (S–PEF) structure, in which only a single PEF $\boldsymbol{f} \triangleq [f[0] \ \ldots \ f[L_f-1]]^T$ is employed jointly for all M transmit antennas, see Fig. 2. This leads to a significant reduction in transmitter complexity.

A. Filter Optimization

As far as filter optimization is concerned, the S–PEF structure leads to an equivalent single–input single–output (SISO) channel model with an effective overall CIR $q_{\text{eff}}[Nn+k_0] \triangleq \sum_{m=1}^{M} q_m[Nn+k_0]$. In the FIR case, the transmit power can thus be expressed as $P = \boldsymbol{f}^H\boldsymbol{\Phi}_{\text{eff}}\boldsymbol{f}$, where $\boldsymbol{\Phi}_{\text{eff}} \triangleq \sum_{m=1}^{M}\boldsymbol{\Phi}_m$. Consequently, utilizing the results in Section III-A, we obtain the optimum FIR PEF $\boldsymbol{f}_{\text{opt}}$ based on (10) by replacing $\boldsymbol{Q}$ by $\boldsymbol{Q}_{\text{eff}}$, $\boldsymbol{\Phi}$ by $\boldsymbol{\Phi}_{\text{eff}}$, and $\boldsymbol{q}$ by $\boldsymbol{q}_{\text{eff}} \triangleq \boldsymbol{Q}_{\text{eff}}^H\boldsymbol{e}_{n_0}$, where $\boldsymbol{Q}_{\text{eff}} \triangleq \sum_{m=1}^{M}\boldsymbol{Q}_m$. Along the same lines, the corresponding minimum error variance is obtained based on (11) by replacing $\boldsymbol{q}$, $\boldsymbol{Q}$, and $\boldsymbol{\Phi}$ by $\boldsymbol{q}_{\text{eff}}$, $\boldsymbol{Q}_{\text{eff}}$, and $\boldsymbol{\Phi}_{\text{eff}}$, respectively.

Similarly, in the IIR case we obtain the frequency response of the optimum IIR PEF, $F_{\text{opt}}(e^{j\omega})$, and the corresponding minimum error variance, by replacing in (17) and (18) $Q_m(e^{j\omega})$, $\Phi_m(e^{j\omega})$, and $X(e^{j\omega})$ by $Q_{\text{eff}}(e^{j\omega}) \triangleq \sum_{m=1}^{M}Q_m(e^{j\omega})$, $\Phi_{\text{eff}}(e^{j\omega}) \triangleq \sum_{m=1}^{M}\Phi_m(e^{j\omega})$, and $X_{\text{eff}}(e^{j\omega}) = |Q_{\text{eff}}(e^{j\omega})|^2/\Phi_{\text{eff}}(e^{j\omega})$, respectively.

B. Comparison

It is of interest to compare the performances of the above S-PEF transmitter structure and the more complex PEF structure discussed in Section III (cf. Fig. 1). To this end, we focus on the IIR case and note that based on the complex version of Hölder's inequality [17] we can establish the following inequality:

$$\left(\sum_{m=1}^{M}|b_m|^2\right)^{1/2}\left(\sum_{m=1}^{M}\left|\frac{a_m}{b_m}\right|^2\right)^{1/2} \ge \left|\sum_{m=1}^{M}a_m\right| \qquad (20)$$

for any $a_m, b_m \in \mathbb{C}$. Substituting $a_m := Q_m(e^{j\omega})$ and $b_m := \sqrt{\Phi_m(e^{j\omega})}$, squaring both sides of (20), and dividing them subsequently by $\sum_{m=1}^{M}\Phi_m(e^{j\omega})$ leads to

$$\underbrace{\frac{\left|\sum_{m=1}^{M}Q_m(e^{j\omega})\right|^2}{\sum_{m=1}^{M}\Phi_m(e^{j\omega})}}_{=X_{\text{eff}}(e^{j\omega})} \le \underbrace{\sum_{m=1}^{M}\frac{|Q_m(e^{j\omega})|^2}{\Phi_m(e^{j\omega})}}_{=X(e^{j\omega})}. \qquad (21)$$

Therefore, since $X(e^{j\omega})$ and $X_{\text{eff}}(e^{j\omega})$ appear in the denominators of the respective error variances, the S–PEF scheme can never outperform the PEF scheme. This is not surprising, since the S–PEF structure may be viewed as a special case of the PEF structure in Fig. 1 with $f_1[n] = \cdots = f_M[n]$, $0 \le n < L_f$. For the special case of an A–pre–Rake filter, $X_{\text{eff}}(e^{j\omega})$ simplifies to

$$X_{\text{eff}}(e^{j\omega}) = \frac{1}{N}\sum_{m=1}^{M}\sum_{k=0}^{N-1}|\tilde{H}_m(e^{j(\omega-2\pi k)/N})|^2 = X(e^{j\omega}), \qquad (22)$$

i.e., in this case the S–PEF and the PEF scheme are equivalent. This equivalence for IIR PEFs and A–pre–Rake filters implies that the S–PEF scheme should perform close to the optimum, as long as a sufficiently long FIR PEF and a good approximation of the A–pre–Rake filter (e.g., an S–pre–Rake filter with a sufficient number of fingers) are employed. Thus, in this case the more complex structure in Fig. 1 can be avoided. On the other hand, if a suboptimum pre–Rake filter with very few fingers and/or short FIR PEFs are used, the PEF structure in Fig. 1 is preferable and will lead to a better performance than the S–PEF structure.

V. Simulation and Numerical Results

In this section, we present computer simulation and numerical results for the proposed PEF schemes for MISO DS–UWB systems. In particular, we show results for the effective SNR at the receiver and the resulting bit error rate (BER). In this context, we consider the practically most relevant cases of $M = 1$ and $M = 2$ transmit antennas and adopt the channel model and system parameters discussed in Section II. In particular, we focus on the CM1 and CM4 channel models, since they have the smallest and the largest average delay spread of the four channel models, respectively. For the case $M = 2$, we assume that the lognormal terms X_m, $m \in \{1, 2\}$, are correlated with a correlation coefficient $\rho = 0.86$ [13].

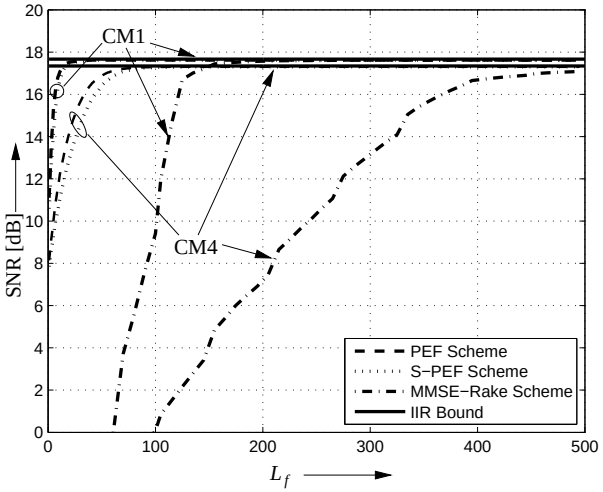

Fig. 3. Average effective SNR vs. L_f for the PEF scheme, the S–PEF scheme, and the MMSE–Rake scheme [9] (UWB channel models CM1 and CM4, A–pre–Rake filters, $M=2$, $N=6$, and $E_b/N_0 = 15$ dB).

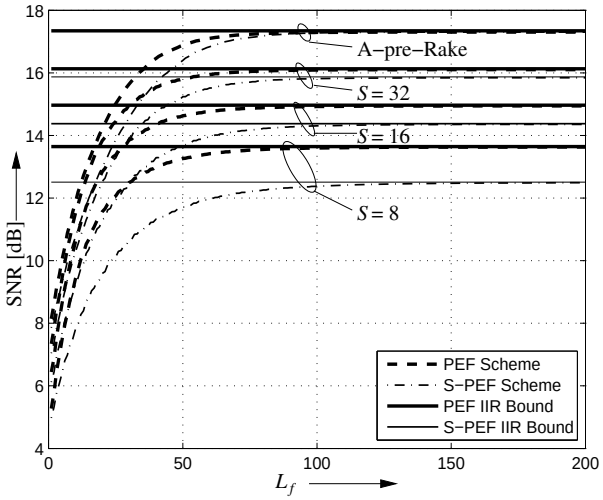

Fig. 4. Average effective SNR vs. L_f for the PEF scheme and the S–PEF scheme (UWB channel model CM4, S–pre–Rake filters with different numbers S of Rake fingers, $M=2$, $N=6$, and $E_b/N_0 = 15$ dB).

A. Effective SNR at the Receiver

Fig. 3 shows the average effective SNR vs. FIR PEF length L_f for the PEF scheme and the S–PEF scheme, respectively, for A–pre–Rake combining, UWB channel models CM1 and CM4, $M=2$ transmit antennas, spreading factor $N=6$, and $E_b/N_0 = 1/\sigma_c^2 = 15$ dB, where E_b and N_0 denote the average energy per bit and the single–sided power spectral density of the underlying passband AWGN process, respectively. The numerical results for the average effective SNR were obtained by averaging (13) over 100 channel realizations, while $\sigma^2_{e,\min}$ was calculated based on the analytical expressions (11) and (18). Fig. 3 shows that as L_f increases, the FIR PEF filters quickly approach the performance of IIR PEF filters (solid lines). Since the average delay spread for CM1 is considerably smaller than for CM4, this convergence is much faster for CM1 than for CM4. We also note that while the PEF scheme achieves a higher SNR than the S–PEF scheme for short FIR PEFs, both schemes achieve the same performance for long FIR and IIR filters, cf. Section IV-B. For comparison, we have also included in Fig. 3 the results for the MMSE–Rake scheme proposed in [9]. As L_f increases, the MMSE–Rake scheme achieves the same performance as the proposed PEF and S–PEF scheme. However, since the filters in the MMSE–Rake scheme operate at the chip level, the convergence to the optimum IIR performance is much slower than for the PEF/ S–PEF scheme. For example, if an SNR of 14 dB is desired for CM4, the PEF scheme and the MMSE–Rake scheme require filter lengths of 18 and 325, respectively. The computation of the long filters required for the MMSE–Rake scheme may be very difficult in practice, even if a recursive (e.g. steepest descent) or an adaptive (e.g. least–mean square) algorithm is used to avoid direct matrix inversion.

In Fig. 4, the performance of the PEF scheme and the S–PEF scheme in conjunction with S–pre–Rake combining using different numbers S of Rake fingers is investigated, for UWB channel model CM4, $M=2$, $N=6$, and $E_b/N_0 = 15$ dB. As predicted in Section IV-B, with S–pre–Rake combining the PEF scheme outperforms the S–PEF scheme even for IIR PEFs, and the performance gap between both schemes increases as the number of fingers decreases. For example, the asymptotic SNR differences between the PEF scheme and the S–PEF scheme for $S=32$, 16, and 8 are 0.25 dB, 0.62 dB, and 1.2 dB, respectively.

B. Bit-Error-Rate Results

Next, we present simulation and numerical results for the BER of the PEF scheme and the S–PEF scheme, where the UWB channel model CM4 is assumed for all results shown in this section. All simulation results presented in the sequel were obtained by averaging over 100 channel realizations. Fig. 5 shows simulated BER results for the PEF scheme and the S–PEF scheme with FIR PEFs of lengths $L_f=5$, 10, and 20, as well as numerical results for the same schemes with IIR PEFs ($M=2$, $N=6$, A–pre–Rake combining). The numerical results for the IIR case were obtained based on a Gaussian approximation of the BER, by utilizing (13) and (18):

$$P_e \approx Q\left(\sqrt{2\left(1/\sigma^2_{e,\min}-1\right)}\right). \tag{23}$$

For comparison, we also show simulation results for the pure A–pre–Rake (or time–reversal) scheme without pre–equalization, as well as the corresponding matched-filter (MF) bound

$$P_{e,\mathrm{MF}} = Q\left(\sqrt{2\mathrm{SNR}_{\mathrm{MF}}}\right), \tag{24}$$

where $\mathrm{SNR}_{\mathrm{MF}} = \frac{1}{\sigma_c^2}\sum_{m=1}^{M}\sum_{k=-\infty}^{\infty}|\tilde{h}_m[k]|^2$, which constitutes an ultimate performance limit for any practical equalization scheme [18]. As can be observed from Fig. 5, both the PEF scheme and S–PEF scheme significantly lower the high BER floor of the pure A–pre–Rake scheme. The performance gap between the PEF scheme and the S–PEF scheme decreases as L_f increases and disappears for $L_f \to \infty$, as expected from the discussion in Section IV-B. We note that even for IIR PEFs there remains a 1–dB gap to the MF bound. However, to further narrow this gap, some form of non–linear processing at the transmitter would be required, which would (further) increase complexity.

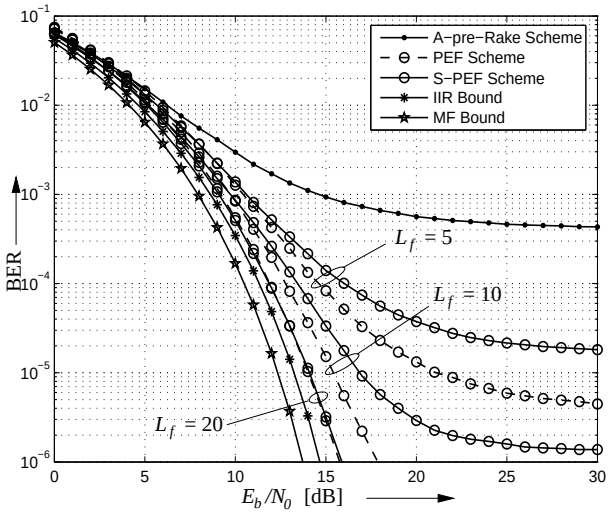

Fig. 5. BER vs. E_b/N_0 for the PEF scheme, the S–PEF scheme, and the pure A–pre–Rake scheme (UWB channel model CM4, A–pre–Rake filters, $M=2$, $N=6$, different filter lengths L_f). The corresponding IIR bound and MF bound are also depicted.

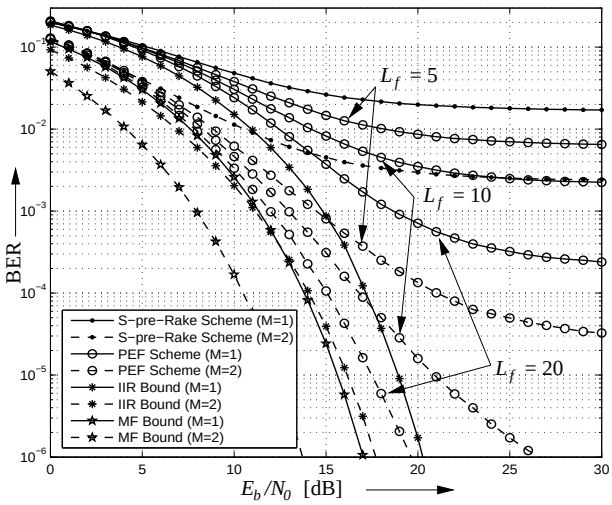

Fig. 6. BER vs. E_b/N_0 for the PEF scheme and the pure S-pre-Rake scheme (UWB channel model CM4, S–pre–Rake filters with $S = 16$ Rake fingers, $M=1, 2$, $N=6$, different filter lengths L_f). The corresponding IIR and MF bounds are also depicted.

In Fig. 6, we compare the performances of the PEF scheme for $M=1$ and $M=2$ transmit antennas, assuming S–pre–Rake combining ($S=16$) and $N=6$. The BER curves for the FIR PEFs and the S–pre–Rake scheme without equalization were simulated, whereas the BER curves for the IIR PEFs as well as the MF bound were again obtained by evaluating (23) and (24), respectively. Fig. 6 shows that a second transmit antenna yields substantial performance improvements, even if the antennas are correlated. This performance gain is about 2.6 dB for IIR PEFs, and even larger gains are obtained for short FIR PEFs. Remarkably, even if we fix the total number of FIR filter taps ML_f, the SISO scheme with $L_f=10$ and $L_f=20$ performs substantially worse than the MISO scheme with $L_f=5$ and $L_f=10$, respectively. The relatively large gap between the MF bounds and the corresponding PEF scheme with IIR filters is due to the suboptimum S–pre–Rake combining.

VI. Conclusions

In this paper, we have proposed two different PEF schemes for MISO DS–UWB systems with pre–Rake combining. The first PEF scheme employs one PEF per transmit antenna, whereas the second, simplified scheme requires only one PEF. In contrast to previously proposed pre–filtering schemes for DS–UWB, both proposed PEF schemes efficiently exploit the channel shortening properties of the pre–Rake filter and operate at the symbol level. Therefore, relatively short PEFs achieve close–to–optimum performance, even for long UWB CIRs. For sufficiently long PEFs and A–pre–Rake combining, both proposed PEF schemes achieve the same performance. However, the S–PEF scheme suffers from a certain performance degradation for suboptimum pre–Rake combining and/or short PEFs. Simulation results have confirmed our analytical findings and the excellent performance of the proposed PEF schemes.

We note that while in this paper only DS–UWB systems have been considered, the proposed PEF schemes are also applicable to other areas of pre–Rake combining, such as TDD–CDMA systems and underwater acoustic communication.

References

[1] R. A. Scholtz, D. M. Pozar, and W. Namgoong. Ultra-Wideband Radio. *EURASIP J. Applied Signal Processing*, 2005:252–272, 2005.

[2] R. Esmailzadeh, E. Sourour, and M. Nakagawa. PreRAKE Diversity Combining in Time-Division Duplex CDMA Mobile Communications. *IEEE Trans. Veh. Technol.*, 48:795–801, May 1999.

[3] A. Parvulescu. Matched-Signal ('MESS') Processing by the Ocean. *J. Acoust. Soc. Am.*, 98:943–960, August 1995.

[4] T. Strohmer, M. Emami, J. Hansen, G. Papanicolaou, and A. Paulraj. Application of Time-Reversal with MMSE Equalizer to UWB Communications. In *Proceedings of the IEEE Global Telecomm. Conf. (Globecom)*, pages 3123–3127, November 2004.

[5] H. Nguyen, I. Kovacs, and P. Eggers. A Time Reversal Transmission Approach for Multiuser UWB Communications. *IEEE Trans. Antennas and Propagation*, 54:3216–3224, November 2006.

[6] Y. Nishida, C. Fukao, M. Fujii, M. Itami, and K. Itoh. A Study on Improving Performance of Pre-Post-RAKE Combining in UWB-IR System. In *Proceedings of the IEEE Intern. Conf. Ultra-Wideband (ICUWB)*, pages 79–84, September 2006.

[7] R. Qiu, C. Zhou, N. Guo, and J. Zhang. Time Reversal With MISO for Ultrawideband Communications: Experimental Results. *IEEE Antennas and Wireless Propagation Letters*, 5:269–273, December 2006.

[8] W. Cao, A. Nallanathan, and C. Chai. On the Tradeoff between Data Rate and BER Performance of Pre-RAKE DS UWB System. In *Proceedings of the IEEE Global Telecomm. Conf. (Globecom)*, November 2006.

[9] M. Emami, M. Vu, , J. Hansen, A. Paulraj, and G. Papanicolaou. Matched Filtering with Rate Back–off for Low Complexity Communications in Very Large Delay Spread Channels. In *Proceedings of the 38th Asilomar Conf. Signals, Systems, and Computers*, pages 218–222, November 2004.

[10] J. Yang and S. Roy. On Joint Transmitter and Receiver Optimization for Multi–Input Multi–Output (MIMO) Transmission Systems. *IEEE Trans. Commun.*, COM-42:3221–3231, December 1994.

[11] R. Fisher, R. Kohno, M. McLaughlin, and M. Welbourn. DS–UWB Physical Layer Submission to IEEE 802.15 Task Group 3a (Doc. Number P802.15-03/0137r4). January 2005.

[12] Channel Modeling Sub-Committee Final Report. IEEE 802.15-02/368r5-SG3a, IEEE P802.15. December 2002.

[13] Z. Lin, X. Peng, K. Png, and F. Chin. Kronecker Modelling for Correlated Shadowing in UWB MIMO Channels. In *Proceedings of the IEEE Wireless Commun. and Networking Conf.*, Hong Kong, March 2007.

[14] A.V. Oppenheim and A.S. Willsky. *Signals and Systems*. Prentice–Hall, Inc., Upper Saddle River, New Jersey, 1996.

[15] T.K. Moon and W.C. Stirling. *Mathematical Methods and Algorithms for Signal Processing*. Prentice Hall, New York, 2000.

[16] B. Hu and N. Beaulieu. Comparison of Modulation Schemes and Rake Receiver Structures for UWB Systems on an IEEE 802.15.3 Indoor Channel. In *Proceedings of the IEEE Global Telecommun. Conf. (Globecom)*, pages 3493–3497, November 2005.

[17] I. S. Gradshteyn and I. M .Ryzhik. *Table of Integrals, Series, and Products*. Academic Press, New York, 2000.

[18] J. G. Proakis, *Digital Communications*, 4th ed. McGraw-Hill, New York, 2001.